ATP and Zn^{2+} induce folding of ALS-associated hSOD1 with fundamentally distinctive mechanisms

Jian Kang, Liangzhong Lim and Jianxing Song*

Department of Biological Sciences, Faculty of Science, National University of Singapore, Republic of Singapore, 119260

*Correspondence to: Jianxing Song, email: dbssjx@nus.edu.sg

Short title: ATP and Zn^{2+} induce folding of hSOD1

J. K. and L.Z.L. contributed equally to this work.
*: to whom correspondence should be addressed. Email: dbssjx@nus.edu.sg.

Competing interests: The authors declare no competing interests.

Abstract

153-residue hSOD1 is first gene whose mutations were identified to cause FALS, while WT-hSOD1 aggregation is linked to SALS. So far >180 ALS-causing mutations have been identified but the underlying mechanism remains an enigma. Mature hSOD1 is stabilized by a disulfide bridge to adopt the Greek-key β-barrel holding zinc and copper cofactors. In contrast, nascent hSOD1 is unfolded and prone to aggregation, which needs Zn2+ at 1:20 to initiate folding into a co-existence of folded and unfolded states. Recently the disruption of Zn2+-binding by mutations was correlated to the acquired ability to form toxic aggregates. Therefore, decoding factors to induce hSOD1 folding provides mechanistic insights and therapy development for hSOD1-associated ALS. Here, by NMR we visualized effects of 12 cations and surprisingly, most including three with Zn2+-like properties had no ability to bind or induce folding. Cu2+ extensively binds but triggers aggregation. Unexpectedly, Fe2+ could induce folding with a Zn2+-like binding pocket. Most unexpectedly, ATP converted nascent hSOD1 into a co-existence of two states at 1:8 with its capacity from triphosphate. By contrast, TMAO showed no detectable conversion even at 1:1000. Comparing conformations and dynamics of ATP- and Zn2+-induced states revealed that hSOD1 maturation requires intrinsic folding capacity encoded by the sequence as well as additional information specifically provided by Zn2+-coordination and disulfide formation. Therefore Zn2+ induces folding by specific coordination but ATP by generally enhancing the intrinsic capacity, as also observed on 140-residue C71G-hPFN1 composed of both α-helices and β-sheets without disulfide bridge. ATP- and Zn2+-induced states without disulfide bridge remain co-existing between two states which are separated by an energy barrier larger than that of C71G-hPFN1. This study unveils the irreplaceable role of Zn2+ in preventing ALS and provides hSOD1-dependent mechanisms for Cu2+/Fe2+ cytotoxicity. Strikingly, ATP appears to induce folding generally, thus rationalizing ageing-dependent onset even for FALS.

Key words: ATP; Cations; human CuZn-superoxide dismutase 1 (hSOD1); Amyotrophic lateral sclerosis (ALS); Protein folding and aggregation; NMR spectroscopy.

Introduction

Amyotrophic lateral sclerosis (ALS) is the most prominent adult motor-neuron disease, clinically characteristic of progressive motor-neuron loss in the spinal cord, brainstem, and motor cortex, which leads to paralysis and death within a few years of onset. ALS was first described in 1869, which affects approximately 1-2 per 100,000 people worldwide (1-3). Most ALS cases are sporadic (90%) (SALS) whereas 10% are familial ALS (FALS). In 1993, human CuZn-superoxide dismutase (hSOD1) was identified to be the first gene associated with FALS (4), and its mutations cause the most prevalent form of FALS, accounting for ~20% of total FALS cases (4-10). hSOD1 is ubiquitously expressed in all tissues and is the most abundant protein in neurons comprising ∼1% of total protein. Currently, >180 mutations have been identified within the 153-residue hSOD1 that are thought to cause ALS by gain of toxicity (http://alsod.iop.kcl.ac.uk/) (9). Intriguingly, aggregation of the wild-type (WT) hSOD1 without any mutations has also been extensively found in SALS patients. So far, despite exhaustive studies, the exact mechanism for hSOD1-associated ALS still remains an enigma (4-10).

hSOD1 represents one of the most studied proteins not only for its physiological and pathological roles, but also for the fundamental principles of the enzymatic catalysis, protein folding and aggregation as well as their modulation by metalation and disulfide bridge formation (4-9). The mature hSOD1 is a homodimeric enzyme of remarkably high stability and solubility, with each subunit folding into an eight-stranded Greek-key β-barrel stabilized by an intramolecular disulfide bridge Cys57-Cys146. Each subunit holds one copper and one zinc ions in close proximity. While zinc ion is coordinated by His63, His71, His80, and Asp83, copper ion is ligated by His46, His48, and His120 (4-9) (Fig. 1A). Previous studies have established that nascent

hSOD1 without metal cofactors and the disulfide bridge folds into the mature form through a very complex multi-step maturation process whose detailed mechanism still remains to be completely elucidated. Nevertheless, it has been well recognized that the critical first step of the maturation is the initial folding of nascent hSOD1 specifically induced by Zn^{2+}, which is followed by the formation of the disulfide bridge and incorporation of copper, both of which need the catalysis by copper chaperone for hSOD1 (CCS) (11-14). In contrast to the mature hSOD1 of very high solubility, the early folding species particularly nascent hSOD1 have very high tendency of aggregation (4-16). Consequently, various super-stable hSOD1 mutants with Cys residues differentially mutated to Ala or/and Ser such as C6A/C111S mutant have been extensively used for biophysical and NMR structural studies (12).

Previously, we have obtained atomic-resolution NMR evidence that L126Z-hSOD1, which has the C-terminal 28 residues truncated and considerably elevated toxicity compared to those with site substitution, was highly disordered without any stable secondary and tertiary structures, as well as lacking of restricted ps-ns backbone motions (15). We further found that nascent hSOD1 was also similarly disordered as L126Z-hSOD1 which is consistent with in-cell studies (11-14), thus providing a biophysical rationale for the observation that WT-hSOD1 is associated with SALS (16). Furthermore, we found that while nascent WT-hSOD1 could bind zinc to undergo the initial folding into the co-existence between the folded and unfolded states at 1:20 (16), L126Z-hSOD1 completely lost the ability to interact with zinc to fold (15). On the other hand, in the absence of Zn, nascent hSOD1 is also able to interact with membranes as L126Z-hSOD1. Nevertheless, upon availability of zinc, nascent hSOD1 becomes co-existing between two states and no longer able to interact with membranes, while L126Z-hSOD1 remains disordered and interacting with membrane (15,16). Remarkably, *in vivo* studies revealed that the ALS-causing mutants of hSOD1 did initiate

ALS pathogenesis by becoming associated with the ER and mitochondria membranes (17). Very recently, a biophysical study showed that the disruption of the ability of hSOD1 by ALS-causing mutations to bind zinc is correlated to the acquired ability to become associated with mitochondria membrane to further form toxic aggregates (18). These results together highlight the extreme criticality of the initial folding of nascent hSOD1, implying that the failure to achieve the initial folding renders WT-hSOD1 to become as toxic as the ALS-causing mutants, thus representing a convergent mechanism for the mutant hSOD1 to cause FALS and WT-hSOD1 to trigger SALS (15,16). In this context, a question of both fundamental and therapeutic importance arises: in addition to zinc cation, are other cations and molecules capable of inducing the initial folding of nascent hSOD1?

In this study, we aimed to address this question by NMR. Briefly we first evaluated the effects of 12 inorganic cations, which include 8 (Na^{+}, K^{+}, Ca^{2+}, Zn^{2+}, Mg^{2+}, Mn^{2+}, Cu^{2+}, and Fe^{2+}) essential for humans (19), 3 (Ni^{2+}, Cd^{2+} and Co^{2+}) widely thought to have physicochemical properties very similar to Zn and previously used to mimic zinc in structure determination (5-8), as well as neurotoxic and environmentally abundant Al^{3+}. Subsequently, we assessed the effect of ATP, the universal energy currency but mysteriously with cellular concentrations of 2-12 mM, which are much higher than required for its classic functions (20). Recently ATP at mM has been increasingly uncovered to energy-independently control protein hemostasis such as to modulate liquid-liquid phase separation (LLPS), to thermodynamically and kinetically inhibit aggregation (21-24) as well as to antagonize the crowding-induced destabilization (25,26). In particular, in the accompanying manuscript on the ALS-causing C71G mutant of human profilin 1 (hPFN1) which co-exists in equilibrium between the folded and unfolded states exchanging at 11.7 Hz, we discovered that ATP could completely convert the unfolded state into the folded state even at 1:2,

while trimethylamine N-oxide (TMAO) well-known to generally induce folding failed to show any detectable conversion even at 1:2000. Very unexpectedly, the inducing capacity of ATP was identified to come from its triphosphate group but the free triphosphate showed strong ability to trigger aggregation (27). However, 140-residue hPFN1 adopts a fold composed of both α-helices and β-sheets without disulfide bridge, as well as already co-exists in two states. So here it is of significant interest to assess whether ATP and triphosphate with physicochemical properties fundamentally different from cations can also induce the initial folding of the completely unfolded nascent state of hSOD1 which adopts a distinctive β-barrel stabilized by one disulfide bridge.

Surprisingly, most of 12 cations show no detectable ability to bind as well as to induce folding of nascent hSOD1 even up to 1:40 beyond which the sample started to precipitate. Intriguingly, Cu^{2+}, the other cofactor of hSOD1, shows extensive binding but triggers severe aggregation. Unexpectedly, Fe^{2+} has been identified for the first time to have the Zn^{2+}-like ability to induce folding with the Fe^{2+}-binding pocket at least partly overlapped with that of Zn^{2+}. Most unexpectedly, ATP has been decoded here to induce folding of nascent hSOD1 into the co-existence between the folded and unfolded states at 1:8 which is physiologically-relevant. As observed on C71G-PFN1 (27), the inducing capacity also comes from its anionic triphosphate group. The free triphosphate can also induce folding of nascent hSOD1 as effectively as ATP but has strong capacity to trigger aggregation. By contrast, TMAO failed to show any detectable inducing capacity even at 1:1000 beyond which the sample started to precipitate. Detailed comparison of NMR conformations and dynamics of the ATP- and Zn-induced folded states unveils that ATP and Zn induce the initial folding of nascent hSOD1 by fundamentally distinctive mechanisms. While Zn initiates folding of nascent hSPD1 by introducing the information additional to the amino acid sequence through specifically coordinating the formation of the Zn-

binding pocket, ATP appears to induce folding by enhancing the intrinsic folding capacity encoded by the sequence, as we also observed on C71G-hPFN1 (27). This study not only unveils the irreplaceable role of Zn2+ in preventing ALS pathogenesis, but also provides hSOD1-dependent mechanisms for Cu2+/Fe2+ cytotoxicity. The present results together with those of C71G-PFN1 (27) imply that ATP may play a previously-unknown role in inducing protein folding, thus shedding light on a long-standing puzzle that even FALS becomes onset only after a certain age, likely when cellular ATP concentrations reduce down to a certain level.

Results

NMR characterization of the Zn-induced folded state.

By exhaustively screening solution conditions including pH, types and concentrations of salts, we have successfully identified the optimized buffer to minimize the aggregation of nascent hSOD1 for high-resolution NMR studies: in 1 mM sodium acetate buffer at pH 4.5. This condition allowed the preparation of soluble and stable hSOD1 samples with a concentration up to 500 μM, which is required to collect high-quality triple-resonance NMR spectra. As hSOD1 of the native sequence contains four cysteine residues, previously we found that they started to form intermolecular disulfide bridges even in the presence of 10 mM DTT once the solution pH was above 5.0, and consequently resulted in immediate precipitation (21,22). Here the low buffer salt concentration (1 mM) is also required to maximize the manifestation of the effects of cations as well as ATP and related molecules.

Completely consistent with in-cell studies (11-14), nascent hSOD1 with the wild-type sequence but without metal cofactors and the disulfide bridge is completely unfolded in the buffer, which has HSQC spectrum with very narrow ^{1}H and ^{15}N spectral dispersions typical of a highly disordered protein (Fig. 1B). This is strikingly different from what was observed on various super-stable pseudo wild-type sequences in which four Cys residues (Cys 6, Cys 57, Cys 111 and Cys 146) were differentially replaced by Ala or Ser to increase stability and inhibit aggregation (12). These super-stable pseudo hSOD1 mutants including the C6A/C111S hSOD1 have been already folded to different degrees in the absence of zinc ion. In particular, upon assing Zn, the C6A/C111S hSOD1 became completely folded with a well-defined three-dimensional structure (Fig. S1A) as determined by NMR (12), which is very similar to the crystal structure of the mature hSOD1 (28).

Strikingly, upon stepwise adding Zn^{2+}, a folded population was formed as unambiguously indicated by the manifestation of a new set of well dispersed HSQC peaks (Fig. 1C). The formation of the folded state is largely saturated at a ratio of 1:20 (hSOD1:Zn) (16) and even with further addition of Zn up to 1:40, the unfolded and folded states still coexist, suggesting that Zn alone is insufficient to completely convert the unfolded population into the folded state, consistent with the in-cell results that the complete formation of the mature WT-hSOD1 structure needs further disulfide formation and copper-load that is catalyzed by human copper chaperone for hSOD1 (hCCS) (10-14). Remarkably, we also showed that the well-dispersed peaks of the folded state became completely disappeared upon adding EDTA at an equal molar concentration of Zn2+, confirming that the formation of the folded state is the Zn^{2}+-induced effect (16).

By analyzing triple-resonance NMR spectra, we have achieved sequential assignments of both folded and unfolded states of hSOD1 in the presence of Zn at 1:20 and Fig. S1B presents their (ΔCα–ΔCβ) chemical shifts, which are the indicators of the secondary structures for both folded and unfolded proteins (29). For the folded state, except for 28 residues Ala1, Gly12, Gly16, Leu42, His46, Gly51-Ala55, Thr58-Ser59, Gly72-Gly73, Asp76-His80, Leu84-Gly85, Asp92, Val118, Glu121-Lys122, Asn131-Glu133 and Gln153 whose HSQC peaks are missing or overlapped (Fig. S1C), all residues have been assigned and many of them have large and negative (ΔCα–ΔCβ) chemical shifts, indicating that Zn^{2+}-induced folded state has well-formed β-sheets. Most convincingly, except for several residues close to the mutation site C6 and C111, the (ΔCα–ΔCβ) chemical shifts of the Zn^{2+}-induced state of nascent WT-hSOD1 are highly similar to those of the Zn^{2+}-induced state of the pseudo-WT-hSOD1 C6A/C111S (Fig. S1C). The results together suggest that in the presence of Zn^{2+}, both nascent WT and pseudo-WT hSOD1 adopt the highly similar β-barrel structures observed on the mature hSOD1 (Fig. S1A). Nevertheless, upon being induced by

Zn^{2+}, the pseudo-WT-hSOD1 became completely folded, while the WT-hSOD1 still has an co-existence of the unfolded and folded states.

We further obtained $\{^{1}H\}-^{15}N$ heteronuclear steady-state NOE (hNOE) of the folded and unfolded states of the WT-hSOD1 in the presence of Zn at 1:20 (Fig. S1D), which reflects the backbone motions on ps-ns time scale (29-32). The residues of the unfolded state have small or even negative hNOE values with an average of -0.11, indicating that it has unrestricted backbone motions on ps-ns time scale. By contrast, most residues of the folded state have positive hNOE values with an average of 0.61, while some are even higher than 0.8, implying that the folded state has highly restricted backbone motions. However, the average hNOE value of the folded state is still smaller than those of well-folded proteins such as EphA4 receptor with an average value of 0.89 (31), but similar to those of the ALS-causing C71G-PFN1 (27) and TDP-43 NTD (32), which also have co-existing unfolded and folded conformations with average hNOE values respectively of 0.70 and 0.71.

Furthermore, we have also collected ^{15}N-edited HSQC-NOESY spectrum on the sample of the WT-hSOD1 in the presence of Zn at 1:20. Indeed, a large number of long-range NOEs has been observed, indicating that the folded state has well-packed tertiary structure. On the other hand, unlike C71G-hPFN1 and TDP-43 NTD which had the co-existence of the unfolded and folded states exchanging respectively at 11.7 Hz (27) and 14 Hz (32), we found no NOE cross-peaks resulting from the exchange between two states, indicating that the time scale for the conformational exchange of two states of the WT-hSOD1 in the presence of Zn at 1:20 is slower than those of C71G-hPFN1 and TDP-43 NTD, In other words, the energy barrier separating two states of the WT-hSOD1 in the presence of Zn at 1:20 is larger than those separating two states of C71G-hPFN1 and TDP-43 NTD (27,32,33).

Furthermore, we also measured the binding of zinc to hSOD1 by isothermal titration calorimetry (ITC) and the heat release was observed upon adding zinc ion, indicating that zinc could indeed bind to nascent hSOD1 (Fig. 1E). However, as the heat changes are expected to result from at least two processes: namely binding of Zn to hSOD1 and binding-induced folding, data fitting is not possible to obtain the thermodynamic parameters for the binding event.

So, an intriguing question arises: why does the WT-hSOD1 still retain an equilibrium between the folded and unfolded forms even in the excess presence of Zn^{2+}? Previous studies revealed a surprising fact that on the one hand, to achieve disulfide formation and copper-load catalyzed by hCCS, the SOD1 needs to populate the folded form bound to Zn^{2+} to some degree. Otherwise, the efficacy of maturation was low (11-14). On the other hand, the interaction between hCCS and_folded SOD1 cannot be too stable but has to be dynamic/transit. If the hSOD1-hCCS complex is too stable, the efficiency of the hCCS-catalyzed maturation will also be reduced or even abolished (11). So the request for dynamic/transit interactions between hSOD1 and hCCS appears to be elegantly fulfilled by the dynamic nature of the immature hSOD1, which at least partly results from the co-existence of the unfolded and folded population in the presence of zinc.

Copper extensively binds but triggers severe aggregation.

We subsequently assessed whether copper, the other cofactor of hSOD1, can bind and induce folding of nascent hSOD1. Intriguingly, on the one hand, as shown in Fig. 2A, Cu^{2+} induced extensive shift and broadening of HSQC peaks of the unfolded state. On the other hand, however, unlike Zn^{2+} which is capable of inducing the manifestation of a complete set of well-dispersed HSQC peaks from the folded state, Cu^{2+} appeared only to induce the formation of a partially-folded state as indicated by the observations that only several well-dispersed HSQC peaks (Fig.

2A) and very up-field 1D peals (Fig. 2B) manifest such as that of Trp32 side chain which are from the folded state. In fact, most well-dispersed HSQC peaks characteristic of the Zn^{2+}-induced folded state were undetectable, implying that a large region of the Cu^{2+}-induced state is not well-folded, or/and undergoes μs-ms conformational exchanges. Interestingly, the Cu^{2+}-induced effect is mostly saturated at 1:6 (hSOD1:Cu^{2+}) as evidenced by the very up-field 1D spectra. The current NMR results are generally consistent with the very recent report that unlike Zn^{2+}, Cu^{2+} has no ability to prevent nascent hSOD1 from interacting with membrane to form toxic aggregates (18), implying that Cu^{2+} has no strong capacity to induce the initial folding of nascent hSOD1, which is required for abolishing the membrane-interacting ability.

We also observed that even upon immediate addition of Cu^{2+}, hSOD1 appeared to undergo μs-ms conformational exchanges or/and dynamic aggregation as evidenced by very broad 1D and HSQC peaks as compared with those in the presence of Zn (Fig. 2A and 2B). Particularly after one hour, the NMR sample in the presence of Cu^{2+} started to form visible aggregates and consequently all NMR signals became disappeared. Consistent with this observation, addition of EDTA to the hSOD1 sample with freshly-added Cu^{2+} could result in the disappearance of very up-field 1D peaks and well-dispersed HSQC peaks, as well as the shifts of HSQC peaks, indicating that the observed effects are specifically induced by Cu^{2+}. However, addition of EDTA to the Cu^{2+}-added hSOD1 sample which was already with visible aggregates failed to solubilize the aggregates as well as to restore the disappeared HSQC peaks.

We managed to conduct ITC titrations of Cu^{2+} into nascent hSOD1 sample at a low protein concentration (5 μM) and the result indicated that Cu^{2+} indeed showed the binding (Fig. 2C). Intriguingly, we also added Cu^{2+} to the hSOD1 sample in the pre-existence of Zn^{2+} at 1:20, but unfortunately the sample got precipitated immediately. In this context, the extensive binding of

Cu^{2+} to the unfolded state, inability to induce the well-folded form, and strong induction of aggregation by Cu^{2+} may partly account for its high *in vivo* toxicity and also rationalize why the delivery and load of copper needs to be specifically implemented by hCCS to the pre-folded hSOD1 population (11-14).

Most cations show no capacity in binding and inducing folding.

So, a question of fundamental and biological interest is whether metal ions other than Zn^{2+} and Cu^{2+} can bind and induce folding of nascent hSOD1. To address this, we have further selected 10 other cations from the periodic table (Fig. S2A), which include Na^{+}, K^{+}, Ca^{2+}, Mg^{2+}, Mn^{2+}, Fe^{2+}, Ni^{2+}, Cd^{2+}, Co^{2+} and Al^{3+} and subsequently conducted titrations into nascent hSOD1 with ratios of cation:hSOD1 reaching up to 1:40 under the exactly same protein concentration and solution conditions used for Zn^{2} as monitored by NMR HSQC spectroscopy, which can detect the binding events at residue-specific resolution with affinities ranging from high to very low events even with Kd of mM (24,34).

Unexpectedly, except for Fe^{2+}, all the cations triggered no considerable shift of HSQC peaks and no manifestation of very up-field 1D and well-dispersed HSQC peaks for nascent hSOD1, as exemplified by the results with Co^{2+}, Ni^{2+}, Cd^{2+}, and Mn^{2+} which induce no large shift of HSQC peaks of nascent hSOD1 even with the ratio reaching up to 1:40 (Fig. S2B), thus suggesting that these cations have no capacity to bind as well as to induce folding of nascent hSOD1.

This is remarkably surprising because previously in various biophysical investigations and structure determinations, Ni^{2+}, Cd^{2+} and Co^{2+} have been widely thought to have physicochemical properties very similar to Zn^{2+} and thus used to substitute Zn^{2+} in the mature SOD1 (5-7). The

present results thus strongly highlight the irreplaceable role of Zn^{2+} in initiating the first step of the maturation: folding of nascent hSOD1. Indeed, previous folding studies have deciphered that zinc appears to uniquely modulate the entire folding free energy surface of hSOD1 (11-14).

Fe^{2+} induces folding to form the folded Fe^{2+}-bound hSOD1

Here by the systematic assessment, for the first time we found that Fe^{2+} owns the capacity in triggering folding of nascent hSOD1 into an equilibrium between the unfolded and folded Fe^{2+}-bound states. So we further conducted a detailed NMR characterization to elucidate its conformational features. As seen in Fig. 3A, addition of Fe^{2+} triggered the manifestation of very up-field 1D and well-dispersed HSQC peaks characteristic of the folded form and the increase in the folded population is mostly saturated at a molar ratio of 1:20 (hSOD1: Fe^{2+}). Fig. 3B presents the superimposition of the HSQC spectra of the Fe^{2+}- and Zn^{2+}-bound hSOD1 forms. Unfortunately, a detailed comparison of the intensities and chemical shifts of NMR peaks induced by Fe^{2+} and Zn^{2+} is impossible because Fe^{2+} has strong paramagnetic effects including effects of relaxation enhancement and pseudo-contact shift (35), which also made the sequential assignment of the Fe^{2+}-bound state impossible by NMR. However, ITC measurement also revealed that Fe^{2+} could indeed bind hSOD1 (Fig. 3C).

Nevertheless, based on the assignments of the Zn^{2+}-bound form, many peaks from the Fe^{2+}-bound hSOD1 are highly superimposable to those of the Zn^{2+}-bound; while some have large differences. Interestingly, as shown in Fig. 3D, the peaks with significant differences are from the residues surrounding the Cu/Zn binding pocket, while the peaks without significant differences are from those located relatively far away from the Cu/Zn binding pocket such as over the β-barrel. This strongly implies that the Fe^{2+}- and Zn^{2+}-bound hSOD1 structures might be very similar

particularly over the β-barrel regions, and further implies that Fe^{2+} binding site is located close to, or even has overlaps with the Cu/Zn binding pocket. Consequently, the residues close to Fe^{2+} showed large differences for their HSQC peaks due to the pseudo-contact shift effect (35), or/and slightly-different conformations in the Fe^{2+}-bound form. Moreover, the up-filed and well-dispersed HSQC peaks also became completely disappeared upon adding EDTA, confirming that the formation of the folded hSOD1 is also Fe^{2+}-induced effect.

We thus conducted a competitive experiment between Zn^{2+} and Fe^{2+} by monitoring the changes of both up-field (Fig. 4A) and HSQC (Fig. 4B and 4C) peaks upon stepwise addition of Zn^{2+} into the hSOD1 sample in the pre-existence of 20x Fe^{2+}. As seen in Fig. 4A, with addition of 10x zinc, the zinc-specific peak in the 1D spectrum manifested. On the other hand, however, as shown in HSQC spectra (Fig. 4B), in the presence of 10x zinc, many HSQC peaks still remain highly similar to those of the Fe^{2+}-bound. Upon addition of 20x Zn^{2+}, although many peaks become superimposable to those of Zn^{2+}-bound form, there are still some peaks more superimposable to those of the Fe^{2+}-bound form (Fig. 4C). This implies that Fe^{2+} and Zn^{2+} binding-sites might be only partly overlapped. Unfortunately, further addition of Zn^{2+} induced severe broadening of the NMR peaks and then visible aggregates of the sample, thus blocking further characterization. Nevertheless, the results of the competitive experiment strongly imply that the presence of Fe^{2+} at high concentrations can interfere in the Zn^{2+}-induced formation of the well-folded hSOD1, which may reduce the efficiency of the hSOD1 maturation.

ATP and PPP induce folding of nascent hSOD1.

Previously, we discovered that ATP could completely convert the unfolded state into the folded state of C71G-hPFN1 even at 1:2 (27). However, C71G-hPFN1 adopt a fold composed of

both α-helices and β-sheets without any disulfide bridge, which already co-exists in equilibrium between the folded and unfolded states with the populations respectively of 55.2% and 44.8% exchanging at 11.7 Hz. So it remains unknow whether ATP can induce folding from the completely unfolded state. In this regard, nascent state of hSOD1 adopting the Greek-key β-barrel provides an excellent model for addressing this question.

Here we titrated ATP into nascent hSOD1 sample as monitored by NMR 1D and HSQC spectroscopy. Upon adding ATP to 1:2, no significant change was observed on 1D (Fig. 5A) and HSQC spectra (Fig. 5B). Unexpectedly, when the ratio was increased to 1:8, well-dispersed HSQC peaks and very up-field 1D signals manifested (Fig. 5A and 5C), as well as further evidenced by the intensity changes at different ratios (Fig. S3). Further addition of ATP even up to 1:20 only led to some slight shifts of HSQC peaks of the unfolded state (Fig. 5D) but up-field 1D peaks from the folded state at 1:20 is highly similar to that at 1:8 only with the intensity slightly reduced (Fig. 5A). However, the addition of ATP beyond 1:20 triggered visible precipitation and resulted in disappearance of NMR signals. The results unambiguously indicates that ATP could indeed induce folding of the completely unfolded nascent hSOD1, and the induction was largely saturated at 1:8, which can be satisfied in most living cells. On the other hand, even at 1:20, ATP could not completely convert the unfolded state into the folded states, indicating that like Zn, ATP also could not completely convert the unfolded population of hSOD1 into the folded state.

We then asked the question which group of ATP has the inducing capacity. To assess this, we first titrated nascent hSOD1 with Adenosine but even with the highest concentrations of 5 mM due to its limited solubility, no large shift of HSQC peaks and no manifestation of up-field 1D signals were detected (Fig. S4), indicating that Adenosine has no detectable ability to induce folding. So we titrated sodium triphosphate (PPP) into nascent hSOD1. Indeed, as we previously

observed on C71G-PFN1, PPP could also induce folding of the unfolded nascent hSOD1. Briefly, very similar to what was observed on ATP, at 1:2, no significant change was observed on HSQC (Fig. 6A) and 1D (Fig. 6B) spectra. However, from 1:4 the folded population was formed with the manifestation of the well-dispersed HSQC and up-field 1D peaks (Fig. 6B, 6C and Fig. S5). Evidently, at 1:8 1D spectra of ATP and PPP were very similar (Fig. 6B), while most HSQC peaks were also superimposable (Fig. 6D), thus suggesting the high similarity of the conformations induced by ATP and by PPP. However, further addition of PPP at 1:10 triggered visible precipitation and resulted in disappearance of NMR signals. This finding indicates that as we observed on C71G-hPFN1 (27), the capacity of ATP to induce folding of nascent hSOD1 also come from its triphosphate group. On the other hand, however, different from ATP which triggered detectable precipitation above 1:20, addition of PPP even to 1:10 is sufficient to triggered severe aggregation.

We have further conducted the titrations with ADP but no folded state was induced even with a ratio up to 1:40 (Fig. S6) above which the sample started to precipitate. Subsequently, we also titrated with sodium pyrophosphate and no induction of folding was detected with the ratio to 1:10 above which the NMR sample started to precipitate. In our previous study on hSOD1 (15,16), we also observed that the extra introduction of sodium phosphate additional to 1 mM phosphate buffer induced no folding but only triggered visible precipitation above 5 mM.

So why do ATP and triphosphate have the very similar capacity in inducing folding of nascent hSOD1 but different abilities in triggering its aggregation? Structurally, ATP is composed of Adenosine and anionic triphosphate group, which is highly negatively charged and thus can exert strong electrostatic screening effect. In this context, for proteins such as nascent hSOD1 which are partially- or highly-disordered with considerable hydrophobic parches exposed,

triphosphate not only can induce folding but also impose the screening effect, which leads to severe aggregation mainly driven by hydrophobic interaction, as we recently observed on the intrinsically disordered TDP-43 PLD containing a hydrophobic segment (36-39) as well as C71G-hPFN1 with the co-existence of the folded and unfolded state (27). Universally, the partially-folded or unfolded proteins with significant exposure of hydrophobic patches are all soluble in unsalted water but become insoluble upon the introduction of salts even at very low concentrations (27,38). Noticeably, nascent hSOD1 is more prone to aggregation than C71G-PFN1 in the presence of the same ratios of ATP and related molecules. This might be partly due to the fact that nascent hSOD1 is completely unfolded and consequently the hydrophobic patches are more exposed to bulk solvent.

Interestingly, as we previously observed on C71G-PFN1, once triphosphate is covalently linked to adenosine to form ATP, on the one hand, ATP still owns the capacity of triphosphate to induce folding but on the other hand its screening effect to trigger the aggregation appears to be reduced to some degree. This might at least result from two possible mechanisms: 1) the screening effect of triphosphate in ATP is attenuated to some degree by interacting with Adenosine; or/and 2) the aromatic base ring of Adenine in ATP may dynamically interact with the exposed hydrophobic patches of the protein, thus serving to shield the hydrophobic patches from the screening effect of triphosphate.

Comparison of NMR conformations and dynamics of the ATP- and Zn-induced folded states.

To compare the solution conformations and dynamics of the ATP- and Zn-induced folded states, we first superimposed their HSQC spectra which were acquired at the same protein concentrations and solution conditions as well as the same temperature (Fig. 7A). While many

HSQC peaks of two states were highly superimposable, some have relatively large differences. Thus, we further collected and analyzed a set of triple-resonance NMR spectra of the ATP-induced state for sequential assignment. Intriguingly, for some residues, although they had detectable HSQC peaks, their Cα and Cβ resonance peaks were undetectable in the triple-resonance HNCACB or even in CBCA(CO)NH experiments. This is reminiscent of what we previously observed on a 38-residue WW1 domain whose HSQC peaks were detectable but no Cα and Cβ peaks were observed for the majority of WW1 residues in HNCACB and CBCA(CO)NH spectra, implying that these residues might undergo conformational exchanges on the microsecond to millisecond time scale (40).

The analysis of triple-resonance spectra led to the assignments of the residues of the ATP-induced folded state of hSOD1 except for 57 residues, which include Ala1, Lys9, Gly12, Asn26-Gly27, Leu38-Thr39, Leu42-His43, Val47-Ala60, Phe64-Asn65. Gly72-His80, Asp90-Asp92, Val103-Leu106, Val119-Glu133, Gln153 (Fig. 7B). Most unassigned residues are located over the loop regions, particularly for those involved in forming the Zn-binding pocket. Nevertheless, for the assigned residues, most of them have (ΔCα–ΔCβ) chemical shifts very similar to those corresponding residues of the Zn-induced state (Fig. 7C). The results suggest that the β-strands of the characteristic β-barrel structure of the mature hSOD1 have been already well-formed in the ATP-induced state, which are also very similar to those of the Zn-induced state. On the other hand, due to the lack of Zn, the loop regions constituting the binding pocket of Zn ion appeared to still undergo intermediate conformational exchanges on the NMR chemical shift time scale and thus became too broad to be undetectable.

We also acquired $\{^{1}H\}$–^{15}N hNOE data of the ATP-induced folded state with an average of 0.59, only slightly smaller than that of the Zn-induced state (0.61) (Fig. 7D). Briefly, the residues

of the β-strands have hNOE values very similar to those corresponding residues of the Zn-induced state. However, Glu40, Gly108 and Gly114 have negative hNOE of -0.21, -0.34 and -0.41 respectively. This result indicates that in the absence of constraints by the Zn-coordination, the residues around the Zn-binding pocket have conformational exchanges on μs-ms time scales. Furthermore, we have collected ^{15}N-edited HSQC-NOESY spectrum on the sample of the ATP-induced state and like the Zn-induced state, no NOE cross-peak was identified to result from the exchange between the unfolded and folded states, indicating that like the Zn-induced state, the time scale for the conformational exchange between the unfolded and folded states in the presence of ATP is slower than that for two states of C71G-hPFN1 (27).

We also attempted to assess whether ATP and zinc together can completely convert the unfolded population into the folded state either by adding ATP into the hSOD1 sample with the pre-existence of zinc at 1:20, or adding Zn into the hSOD1 sample with the pre-existence of ATP at 1:8. Interestingly, both up-field 1D (Fig. 8A) and HSQC (Fig. 8B) peaks of two resulting hSOD1 samples became very similar, as well as similar to those of hSOD1 sample only in the presence of zinc at 1:20. The results imply that the major difference between the ATP- and Zn-induced folded states are over the loop regions as reflected by ($\Delta C\alpha - \Delta C\beta$) chemical shifts (Fig. 7C). Upon further addition of Zn into the hSOD1 sample with the pre-existence of ATP, the major conformational change is over the loop regions which become folded as contrasted by the Zn-coordination.

Furthermore, in ^{15}N-edited HSQC-NOESY spectrum of the hSOD1 sample in the presence of ATP at 1:8 and Zn at 1:20, again no NOE cross-peak was identified to result from the exchange between the unfolded and folded states, implying that even in the presence of both ATP and Zn, the two states are still separated by a large free-energy barrier.

TMAO failed to induce the folding but triggered aggregation.

Currently, trimethylamine N-oxide (TMAO) is well-established to have the general capacity in inducing protein folding (41,42). Therefore, we titrated TMAO into nascent hSOD1 sample. As shown in Fig. 9, at ratios from 1:2 to 1:20, no large shift was observed for HSQC peaks of nascent hSOD1. At 1:100, many peaks showed large shifts but no well-dispersed peaks manifested. Even at 1:1000, the majority of HSQC peaks underwent large shifts but still no up-field 1D and well-dispersed HSQC peaks manifested. On the other hand, at 1:1000, the NMR peaks became broad and the sample become completely precipitated after one hour and NMR signals became disappeared. The results unambiguously revealed that unlike ATP and zinc ion, TMAO was unable to induce the folding of nascent hSOD1 even with the ratio up to 1:1000. This is consistent with our results on C71G-hPFN1 (27) and previous reports that TMAO concentrations needed to reach ~M to induce the folding of proteins (41,42). Unfortunately for aggregation-prone C71G-hPFN1 and nascent hSOD1, the polar TMAO molecules could still induce aggregation at such high concentrations.

Discussion

Despite exhaustive studies on hSOD1, here by a systematic assessment we uncovered a surprising finding: in contrast to the widespread belief, the majority of 12 cations have no Zn^{2+}-like ability to bind as well as to induce folding of nascent hSOD1. In particular, Ni^{2+}, Cd^{2+} and Co^{2+}, which have been widely believed to have physicochemical properties very similar to Zn^{2+} and thus utilized to substitute Zn^{2+} in the mature hSOD1 for various biophysical and structural studies (5-7), also have no detectable ability to bind as well as to induce the initial folding. The finding thus highlights the extremely-critical role of zinc in switching the toxic nascent hSOD1 associated with SALS into the non-toxic folded state, consistent with the in-cell observation (43). Indeed, increasing evidence implies that abnormal zinc homeostasis is related to ALS pathogenesis and to increase the effective cellular concentration of zinc such as by the dietary intake might offer an important therapy for SALS patients caused by WT hSOD1 (44).

Intriguingly, although Cu^{2+}, the other cofactor of hSOD1, shows extensive binding to nascent hSOD1. it only has weak capacity in inducing folding but owns strong ability to trigger severe aggregation. Therefore, Zn^{2+} appears to be selected by nature to serve as the cofactor of hSOD1 not only because it is just a positively charged cation, but it owns a unique integration of at least three abilities: 1) to specifically coordinate the formation of the Zn^{2}-binding pocket and; 2) to induce the initial folding of nascent hSOD1 as well as; 3) to occupy the pocket of mature hSOD1 to serve as a cofactor for enzymatic functions. In this context, while Ni^{2+}, Cd^{2+} and Co^{2+} have the ability to bind the finally formed Zn^{2}-binding pocket in mature hSOD1, which needs the stabilization by the covalently cross-linked disulfide bridge Cys57-Cys146, they completely lack the Zn^{2+}-like ability to specifically coordinate the formation of the Zn^{2}-binding pocket and to induce the initial folding of nascent hSOD1. On the other hand, although Cu^{2+} can site in a pocket

in the mature hSOD1 to serve as a cofactor as well as extensively bind nascent hSOD1, it has very weak capacity in inducing folding but exerts a strong adverse effect to trigger severe aggregation, which may rationalize why the free Cu^{2+} ion is highly toxic in cells and as such the human copper chaperone for hSOD1 (hCCS) is absolutely needed to carry and then load Cu^{2+} to hSOD1 (11-14).

Here, for the first time Fe^{2+} has been identified to have the Zn^{2}-like ability to induce folding of nascent hSOD1 with the binding pocket at least partly overlapped with that for Zn^{2+}. As no previous study has shown that the Fe^{2+}-bound hSOD1 is compatible for further formation of the disulfide bridge and load of Cu^{2+} catalyzed by hCCS to form biologically active Fe^{2+}-bound hSOD1 in cells. Consequently Fe^{2+} behaves to compete with Zn^{2+} in binding hSOD1 and thus intervene in the first step of the hSOD1 maturation. This finding may uncover a previously unknown mechanism for the iron toxicity in cells by directly targeting hSOD1. Briefly, hSOD1 functions as a central antioxidant enzyme to remove the superoxide free radical responsible for oxidative stress, which has been increasingly identified to cause various human diseases, particularly neurodegenerative diseases including ALS (45-48). Iron appears to be a double-edged sword: it is the most abundant "trace element" absolutely required for humans' survival, but high levels of free iron ion can quickly lead to cell death. Under the normal conditions, the cellular concentration of free iron is very low, but under the pathological conditions such as the breakdown of the blood-central nerve system characteristic of neurodegenerative diseases and aging, the concentration of the blood-derived iron can reach very high. Indeed, iron is accumulated in various neurodegenerative as well as other diseases but the underlying mechanisms for its toxicity still remain to be fully elucidated (45-54). Currently, iron is well-known to act as a notorious accelerator for oxidative stress through its reactivity with peroxide, thus generating the highly reactive hydroxyl radical by Fenton chemistry (45). In light of the present finding, iron might also

manifest its cellular toxicity by interfering in the maturation of hSOD1. The results may also explain the beneficial effects on reducing the risk of neurodegenerative diseases by antioxidant natural products such as flavonoids which have EDTA-like chelating activity to clean up free copper and irons in brains (55,56).

Most unexpectedly, ATP/triphosphate with physicochemical properties fundamentally-different from inorganic cations also have the capacity in inducing the initial folding of nascent hSOD1 at a ratio of 1:8, which is even lower than that of Zn^{2+} at 1:20. By contrast, TMAO failed to induce detectable folding even with the ratio up to 1:1000. The detailed comparison of conformations and dynamics of the ATP- and Zn-induced folded states implies that for the WT-hSOD1 sequence, its complete maturation at least needs: 1) the intrinsic folding capacity encoded by the amino acid sequence; 2) additional information provided by Zn-specific coordination, 3) disulfide formation and load of Cu^{2+} catalyzed by hCCS. It appears that fundamentally different from the positively-charged Zn^{2+} ion which induces folding by providing the information additional to the amino acid sequence, the highly negatively-charged ATP and triphosphate act to induce the initial folding by enhancing the intrinsic folding capacity encoded by the sequence as we proposed for the ATP-induced folding of C71G-PFN1 (27). As such, only the β-barrel structure is well-formed in the ATP-induced folded state while the loops involved in the Zn^{2+}-binding pocket still undergo μs-ms conformational exchanges, because the formation of the Zn^{2+}-binding pocket needs the additional information not encoded in the sequence but provided by the Zn-specific coordination.

For the special case of hSOD1, its Cys residues appear to carry the key information to specify the complete folding of hSOD1. The lack of the disulfide bridge renders both ATP- and Zn-induced folded states to have an co-existence of the folded and unfolded states, which are

separated by the energy barrier larger than that separating two states of C71G-PFN1 (27). In this context, the mutation of Cys to Ser and Ala in the super-sable C6A/C111S mutant appears to reduce the barrier and consequently the C6A/C111S mutant becomes completely folded without the existence of the unfolded state upon induction by Zn (12). This observation is of fundamental interest to protein folding, which implies the possibility that kinetic barriers involved in Cys residues might play a key role in the folding process of hSOD1, as observed on other proteins such as Cathepsin B (57,58). Previously it has been shown that the mature well-folded Cathepsin B with the removal of its propeptide essential for its initial folding loses the ability to spontaneously refold back to the well-folded state and becomes precipitated if the mature Cathepsin B was unfolded such as by neutral pH buffers and urea (58). Intriguingly, however, previously we have found that once the active-site residue Cys29 was mutated to Ser, the mature Cathepsin B mutant suddenly become capable of spontaneously refolding back to the well-folded native structure after unfolding, implying that Cys29 plays a key role in constituting the kinetic barrier during its folding (58).

In light of the results that ATP/triphosphate can induce folding of both C71G-PFN1 (27) and nascent hSOD1 which have unrelated sequences and functions as well as adopt distinctive folds and exist at different stages of folding, here we propose a potential mechanism as previously (27). Briefly, even without needing of strong and specific binding, ATP and triphosphate have been found to effectively interact with the protein hydration of both intrinsically-disordered and well-folded proteins (21-27,59). On the other hand, water molecules hydrogen bonded with protein atoms, particularly with backbone atoms have been established to play a key role in controlling protein folding equilibrium (60-62). As such, once the water molecules critical for folding interact with ATP/triphosphate, their hydrogen-bonds with protein backbone atoms are anticipated to

become weakened or even dissociated. Consequently, the protein backbone atoms will switch to forming intramolecular hydrogen bonds which acts to drive the conversion from the unfolded state into the folded state (27,60-62).

Strikingly, triphosphate has been previously proposed to be the key intermediate for prebiotic chemistry in evolution (63,64). Our current study thus implies that nature selected triphosphate as the key intermediate also because of its high efficiency in inducing protein folding. However, due to its strong ability to exert screening effect to trigger aggregation for the unfolded or partially-unfolded states of proteins as exemplified by nascent hSOD1 and C71G-PFN1 here as well as CHABII (65-67) as well as TDP-43 NTD (68), in most modern cells, the concentrations of triphosphate become extremely low. Nevertheless, it has been found that in some single-cell organisms, inorganic polyphosphates still function as a primordial chaperone, but the underlying mechanism remains elusive (69,70). Here we propose that polyphosphates might share the same mechanism of triphosphate to enhance protein folding.

ATP appears to still operate at fundamental levels in modern cells to energy-dependently control protein homeostasis together with the energy-dependent chaperone and disaggregase machineries. This capacity might be particularly important for preventing toxic misfolding and aggregation of proteins with the destabilizing mutants which can cause human diseases This may rationalize the long-standing puzzle that the risk of neurodegenerative diseases such as FALS dramatically increases with being aged, which is characterized by the constant reduction of ATP concentrations.

Materials and methods

Chemicals and preparation of the recombinant hSOD1 protein

ATP, ADP, Adenosine, sodium tripolyphosphate (PPP), sodium pyrophosphate (PP) and trimethylamine N-oxide (TMAO) as well as chloride salts of 12 cations were all purchased from Sigma-Aldrich as previously reported (21-24).

The gene encoding the wild-type hSOD1 of the native sequence was purchased from Genscript with *E. coli* preferred codons (15,16). To remove the inference of extra residues, the gene was subsequently cloned into a modified vector pET28a without any tag (16). Then the expression vector was transformed into and overexpressed in *Escherichia coli* BL21 (DE3) cells (Novagen). The recombinant hSOD1 protein was found in inclusion body. As a result, the pellets were first washed with buffers several times and then dissolved in a phosphate buffer (pH 8.5) containing 8 M urea and 100 mM dithiothreitol (DTT) to ensure complete conversion to Cys-SH. After 1 hour, the solution was acidified by adding 10% acetic acid and subsequently purified by reverse-phase (RP) HPLC on a C4 column eluted by water-acetonitrile solvent system (15,16). The HPLC elution containing pure recombinant hSOD1 was lyophilized and stored at -80 degree.

The generation of isotope-labeled proteins for NMR studies followed a similar procedure except that the bacteria were grown in M9 medium with the addition of $(^{15}NH_4)_2SO_4$ for ^{15}N labeling and $(^{15}NH_4)_2SO_4$ /[^{13}C]-glucose for ^{15}N-/^{13}C-double labelling (15,16). The purity of the recombinant proteins was checked by SDS–PAGE gels and verified by a Voyager STR matrix-assisted laser desorption ionization time-of-flight-mass spectrometer (Applied Biosystems), as well as NMR assignments. The concentration of protein samples was determined by the UV spectroscopic method in the presence of 8 M urea (15,16,71,72).

As hSOD1 of the native sequence is highly prone to aggregation, previously, we have exhaustively screened buffer conditions including salt types and concentrations (15,16) and successfully found the optimized buffer conditions: 1 mM sodium acetate buffer with the final pH adjusted to 4.5. As such, here hSOD1 protein, chloride salts of 12 cations ATP and related molecules were all prepared in 1 mM sodium acetate-d_3 buffer with the final pH adjusted to 4.5 by very diluted NaOH or HAc.

ITC experiments

Isothermal titration calorimetry (ITC) experiments were performed using a Microcal VP isothermal titration calorimetry machine as described previously (40). The hSOD1 at a concentration of 5 μM was placed in a 1.8-ml sample cell, and each salt at a concentration of 6 mM were loaded into a 300-μl syringe. The samples were first degassed for 15 min to remove bubbles before the titrations were initiated. Control experiments with the same parameter settings were also performed for each inorganic salt without hSOD1, to subtract the effects because of sample dilution.

NMR experiments

All NMR experiments were acquired at 25 degree on an 800 MHz Bruker Avance spectrometer equipped with pulse field gradient units as described previously (15,16). To achieve sequential assignments, triple resonance NMR spectra HN(CO)CACB and CBCA(CO)NH were collected on the ^{15}N-/^{13}C- double labeled hSOD1 samples while {^{1}H}–^{15}N heteronuclear steady-state NOE (hNOE) and HSQC-NOESY spectra were collected on the ^{15}N-labeled samples. NMR

^{1}H chemical shifts were referenced to external DSS at 0.0 ppm (15,16). NMR spectra were processed with NMR Pipe (73) and analyzed with NMR View (74).

For NMR titrations of 12 cations, ^{15}N-labelled hSOD1 samples at a protein concentration of 50 μM in 1 mM sodium acetate-d3 buffer at pH 4.5 were used with stepwise additions of each cation at molar ratios of 1:0.5, 1:1, 1:2, 1:4, 1:6, 1:8, 1:10, 1:12, 1:16, 1:20, 1:24, 1:30 and 1:40. For NMR titrations of ATP and related molecules, ^{15}N-labelled hSOD1 samples at a protein concentration of 50 μM were used with stepwise additions of ATP/PPP at molar ratios of 1:0.5, 1:1, 1:2, 1:4, 1:8, 1:12, 1:20, 1:24 and 1:30. For Adenosine, ^{15}N-labelled hSOD1 samples at a protein concentration of 50 μM were used with stepwise additions of 1:0.5, 1:8, 1:20, 1:40, 1:60 and 1:100. For ADP/PP, 1:0.5, 1:4, 1:8, 1:12, 1:20, 1:30, 1:40 and 1:50.

Acknowledgements

This study is supported by Ministry of Education of Singapore MOE Tier 1 A-8000711-00-00 Grant to Jianxing Song.

Author contributions

J.S. designed research; J. K., L. L. and J.S. performed research; J. K.; L.L. and J.S. analyzed data; J.S. wrote the paper.

References

1. L. I. Bruijn, T. M. Miller, D. W. Cleveland, Unraveling the mechanisms involved in motor neuron degeneration in ALS. *Annu. Rev. Neurosci*. **27,** 723–749 (2004).

2. M. C. Kiernan, et al. Amyotrophic lateral sclerosis. *Lancet*, **377,** 942–955 (2011).

3. B. V. Zlokovic, Neurovascular pathways to neurodegeneration in Alzheimer's disease and other disorders. *Nat Rev Neurosci* **12,** 723–738 (2011).

4. D. R. Rosen, et al. Mutations in Cu/Zn superoxide dismutase gene are associated with familial amyotrophic lateral sclerosis. *Nature*. **362,** 59-62 (1993).

5. Y. Sheng, et al. Superoxide dismutases and superoxide reductases. *Chem Rev*. **114,** 3854-918 (2014).

6. J. S. Valentine, P. A. Doucette, S. Zittin Potter, Copper-zinc superoxide dismutase and amyotrophic lateral sclerosis. *Annu Rev Biochem*. **74,** 563-93 (2005).

7. G. S. A. Wright, S. V, Antonyuk, S. S. Hasnain The biophysics of superoxide dismutase-1 and amyotrophic lateral sclerosis. *Q Rev Biophys*. 52, e12 (2019).

8. J. Huai, Z. Zhang, Structural Properties and Interaction Partners of Familial ALS-Associated SOD1 Mutants. *Front Neurol.* 10, 527 (2019)

9. O. Abel, et al. ALSoD: A user-friendly online bioinformatics tool for amyotrophic lateral sclerosis genetics. *Hum Mutat.* **33,** 1345-1351 (2012).

10. F. Chiti, C. M. Dobson, Protein misfolding, functional amyloid, and human disease. *Annu. Rev. Biochem.* 75, 333–366 (2006).

11. L. Banci, et al. Human superoxide dismutase 1 (hSOD1) maturation through interaction with human copper chaperone for SOD1 (hCCS). *Proc Natl Acad Sci U S A.* **109,** 13555-13560 (2012).

12. L. Banci, et al. Human SOD1 before harboring the catalytic metal: solution structure of copper-depleted, disulfide-reduced form. *J Biol Chem.* **281,** 2333-2337 (2006).

13. L. Banci, et al. Atomic-resolution monitoring of protein maturation in live human cells by NMR. *Nat Chem Biol*. **9,** 297-9 (2013).

14. E. Luchinat, et al. In-cell NMR reveals potential precursor of toxic species from SOD1 fALS mutants. *Nat Commun*. **5,** 5502 (2014).

15. L. Lim, X. Lee, J. Song, Mechanism for transforming cytosolic SOD1 into integral membrane proteins of organelles by ALS-causing mutations. *Biochim Biophys Acta*. **1848,** 1-7 (2015).

16. L. Lim, J. Song, SALS-linked WT-SOD1 adopts a highly similar helical conformation as FALS-causing L126Z-SOD1 in a membrane environment. *Biochim Biophys Acta.* **1858,** 2223-30 (2016).

17. S. Sun et al. Translational profiling identifies a cascade of damage initiated in motor neurons and spreading to glia in mutant SOD1-mediated ALS. *Proc Natl Acad Sci U S A.* **112,** E6993-7002 (2015).

18. A. Sannigrahi, et al. The metal cofactor zinc and interacting membranes modulate SOD1 conformation-aggregation landscape in an in vitro ALS model. *Elife.* 10, e61453 (2021)

19. C. G. Fraga, Relevance, essentiality and toxicity of trace elements in human health. *Mol Aspects Med.* **26,** 235-44 (2005).

20. A. Leningher, Principles of Biochemistry. New York: W. H. Freeman and Company; 2005

21. A. Patel, et al. ATP as a biological hydrotrope. *Science.* **356,** 753–756 (2017).

22. A. M. Rice, M. K. Rosen, ATP controls the crowd. *Science.* **356,** 701–702 (2017).

23. J. Kang, et al. A unified mechanism for LLPS of ALS/FTLD-causing FUS as well as its modulation by ATP and oligonucleic acids. *PLoS Biol.* **17,** e3000327 (2019).

24. J. Kang, L. Lim, J. Song, ATP binds and inhibits the neurodegeneration-associated fibrillization of the FUS RRM domain. *Commun Biol*. **2,** 223 (2019).

25. Y. He, J. Kang, J. Song, ATP antagonizes the crowding-induced destabilization of the human eye-lens protein γS-crystallin. *Biochem Biophys Res Commun*. 526, 1112-1117 (2020).

26, J. Song, ATP energy-independently controls protein homeostasis with unique structure and diverse mechanisms. *Protein Science,* **30,** 1277-1293 (2021).

27. J. Kang, L. Lim, J. Song, ATP energy-independently induces folding of ALS-causing C71G-hPFN1.

28. R. W. Strange, et al. Variable metallation of human superoxide dismutase: atomic resolution crystal structures of Cu-Zn, Zn-Zn and as-isolated wild-type enzymes. *J Mol Biol.* **356,** 1152-62 (2006).

29. H. J. Dyson, P. E. Wright Unfolded proteins and protein folding studied by NMR. *Chem Rev* **104,** 3607–3622 (2004).

30. O. Zhang, et al. Backbone 1H and 15N resonance assignments of the N-terminal SH3 domain of drk in folded and unfolded states using enhanced-sensitivity pulsed field gradient NMR techniques. *J Biomol NMR* **4,** 845–858 (1994).

31. H. Qin, L. Z. Lim, J. Song. Dynamic principle for designing antagonistic/agonistic molecules for EphA4 receptor, the only known ALS modifier. *ACS Chem Biol*. 10, 372-8 (2015).

32. H. Qin, et al. TDP-43 N terminus encodes a novel ubiquitin-like fold and its unfolded form in equilibrium that can be shifted by binding to ssDNA. *Proc Natl Acad Sci U S A*. **111,** 18619-24 (2014).

33. A.G. Palmer, C. D. Kroenke, J. P. Loria, Nuclear magnetic resonance methods for quantifying microsecond-to-millisecond motions in biological macromolecules. *Methods Enzymol* 339, 204–238 (2001).

34. M. P. Williamson, Using chemical shift perturbation to characterise ligand binding. *Prog Nucl Magn Reson Spectrosc.* 73, 1-16 (2013).

35. G. Otting, Protein NMR using paramagnetic ions. *Annu Rev Biophys*. **39,** 387-405 (2010).

36. M. Dang, et al. ATP biphasically modulates LLPS of TDP-43 PLD by specifically binding arginine residues. *Commun Biol.* 4, 714 (2021).

37. M. Dang, et al. Arg/Lys-containing IDRs are cryptic binding domains for ATP and nucleic acids that interplay to modulate LLPS. *Commun Biol*. 5, 1315 (2022).

38. J. Song, Insight into "insoluble proteins" with pure water. *FEBS Lett.* 583, 953-959 (2009).

39. J. Song, Why do proteins aggregate? “Intrinsically insoluble proteins” and “dark mediators” revealed by studies on “insoluble proteins” solubilized in pure water. *F1000Research*. 2: 94 (2013).

40. H. Qin, et al. Identification and structural mechanism for a novel interaction between a ubiquitin ligase WWP1 and Nogo-A, a key inhibitor for central nervous system regeneration. *Biochemistry.* 47, 13647-58 (2008).

41. I. Baskakov, D. W. Bolen, Forcing thermodynamically unfolded proteins to fold. *J Biol Chem.* 273, 4831-4834 (1998).

42. Y. T. Liao, *et al.,* Trimethylamine N-oxide stabilizes proteins via a distinct mechanism compared with betaine and glycine. *Proc Natl Acad Sci U S A.* ***114,*** 2479-2484 (2017).

43. K. Homma, et al., SOD1 as a molecular switch for initiating the homeostatic ER stress response under zinc deficiency, **Mol. Cell 52,** 75–86 (2013).

44. H. F. Lopes da Silva, et al., Dietary intake and zinc status in amyotrophic lateral sclerosis patients. *Nutr Hosp.* 34, 1361-1367 (2017).

45. B. Halliwell, J.M.C. Gutteridge, Free Radicals in Biology and Medicine, 3rd ed., Oxford Univ. Press, Oxford, (1999).

46. N. A. Simonian, J. T. Coyle, Oxidative stress in neurodegenerative diseases. *Annu Rev Pharmacol Toxicol.* **36,** 83-106 (1996).

47. S. C. Barber, R. J. Mead, P. J. Shaw Oxidative stress in ALS: a mechanism of neurodegeneration and a therapeutic target. *Biochim Biophys Acta*. **1762,** 1051-67 (2006).

48. E. A. Winkler, et al., Blood-spinal cord barrier disruption contributes to early motor-neuron degeneration in ALS-model mice. *Proc Natl Acad Sci U S A*. **111,** E1035-42 (2014).

49. N. C. Andrews, P. J. Schmidt Iron homeostasis. *Annu Rev Physiol*. **69,** 69-85 (2007).

50. T. A. Rouault Iron metabolism in the CNS: implications for neurodegenerative diseases. *Nat Rev Neurosci.* **14,** 551-64 (2013).

51. K. Joppe, et al. The Contribution of Iron to Protein Aggregation Disorders in the Central Nervous System. *Front Neurosci*. **13,** 15 (2019).

52. A. Montagne, et al., Blood-brain barrier breakdown in the aging human hippocampus. *Neuron*. **85,** 296-302 (2015).

53. P. T. Ronaldson, T. P. Davis. Targeting Transporters: Promoting Blood-brain barrier repair in Response to Oxidative Stress Injury. *Brain Res*. doi: 10.1016/j.brainres.2015.03.018 (2015).

54. A. Ignjatović, et al., Brain iron MRI: a biomarker for amyotrophic lateral sclerosis. *J Magn Reson Imaging*. **38,** 1472-9 (2013).

55. X. Wang, et al. Role of Flavonoids in the Treatment of Iron Overload. *Front Cell Dev Biol.* 9, 685364 (2021).

56. E. Rodríguez-Arce, M. Saldías, Antioxidant properties of flavonoid metal complexes and their potential inclusion in the development of novel strategies for the treatment against neurodegenerative diseases. *Biomed Pharmacother* 143, 112236 (2021).

57. D. Baker, D. A. Agard, Kinetics versus thermodynamics in protein folding. *Biochemistry.* **33,** 7505-9 (1994).

58. J. Song, et al. The active-site residue Cys-29 is responsible for the neutral-pH inactivation and the refolding barrier of human cathepsin B. *EBS Lett.* **475,** 157-162 (2000).

59. M. Nishizawa, *et al.,* Effects of Weak Nonspecific Interactions with ATP on Proteins. *J Am Chem Soc.* **143,** 11982-11993 (2021).

60. R. L. Baldwin, New directions in the study of Peptide h-bonds and Peptide solvation. *Adv. Protein Chem.* **72,** ix–xi (2005).

61. G. D. Rose, P. J. Fleming, J. R. Banavar, A. Maritan, A backbone-based theory of protein folding. *Proc Natl Acad Sci U S A.* **103,** 16623-16633 (2006).

62. E. T. Powers, S. Deechongkit, J. W. Kelly, Backbone-Backbone H-Bonds Make Context-Dependent Contributions to Protein Folding Kinetics and Thermodynamics: Lessons from Amide-to-Ester Mutations. *Adv Protein Chem.* **72,** 39-78 (2005).

63. F. H. Westheimer, Why nature chose phosphates. *Science.* **235,** 1173-1178 (1987)/

64. S. C. Kamerlin SC, et al. Why nature really chose phosphate. *Q Rev Biophys*. 46, 1–132 (2013).

65. J. Song *et al.,* NMR solution structure of a two-disulfide derivative of charybdotoxin: structural evidence for conservation of scorpion toxin alpha/beta motif and its hydrophobic side chain packing. *Biochemistry.* 36, 3760-3766 (1997).

66. J. Song *et al.,* A gradual disruption of tight side-chain packing: 2D 1H-NMR characterization of acid-induced unfolding of CHABII. *Nat Struct Biol.* ***6,*** 129–134 (1999).

67. Z. Wei, J. Song, Molecular mechanism underlying the thermal stability and pH-induced unfolding of CHABII. *J Mol Biol.* **348,** 205-18 (2005).

68. L. Wang, J. Kang, L. Lim, et al, TDP-43 NTD can be induced while CTD is significantly enhanced by ssDNA to undergo liquid-liquid phase separation. Biochem Biophys Res Commun. 499, 189–195 (2018).

69. M. J. Gray, et al. Polyphosphate is a primordial chaperone. *Mol Cell*. **53,** 689–699 (2014).

70. N. N. Rao, et al.. Inorganic polyphosphate: Essential for growth and survival. *Annu Rev Biochem*. **78,** 605–647 (2009).

71. C. N. Pace *et al.,* How to measure and predict the molar absorption coefficient of a protein. *Protein Sci.* **4,** 2411–2423 (1995).

72. M. Li, *et al.,* Structural characterization of the human Nogo-A functional domains. *The FEBS Journal.* 271, 3512-3522 (2004).

73. F. Delaglio et al., NMRPipe: a multidimensional spectral processing system based on UNIX pipes. *J. Biomol. NMR*. **6,** 277–293 (1995).

74. B. A. Johnson, R. A. Blevins, NMR view: a computer program for the visualization and analysis of NMR data. *J. Biomol. NMR*. **4,** 603–614 (1994).

Figures

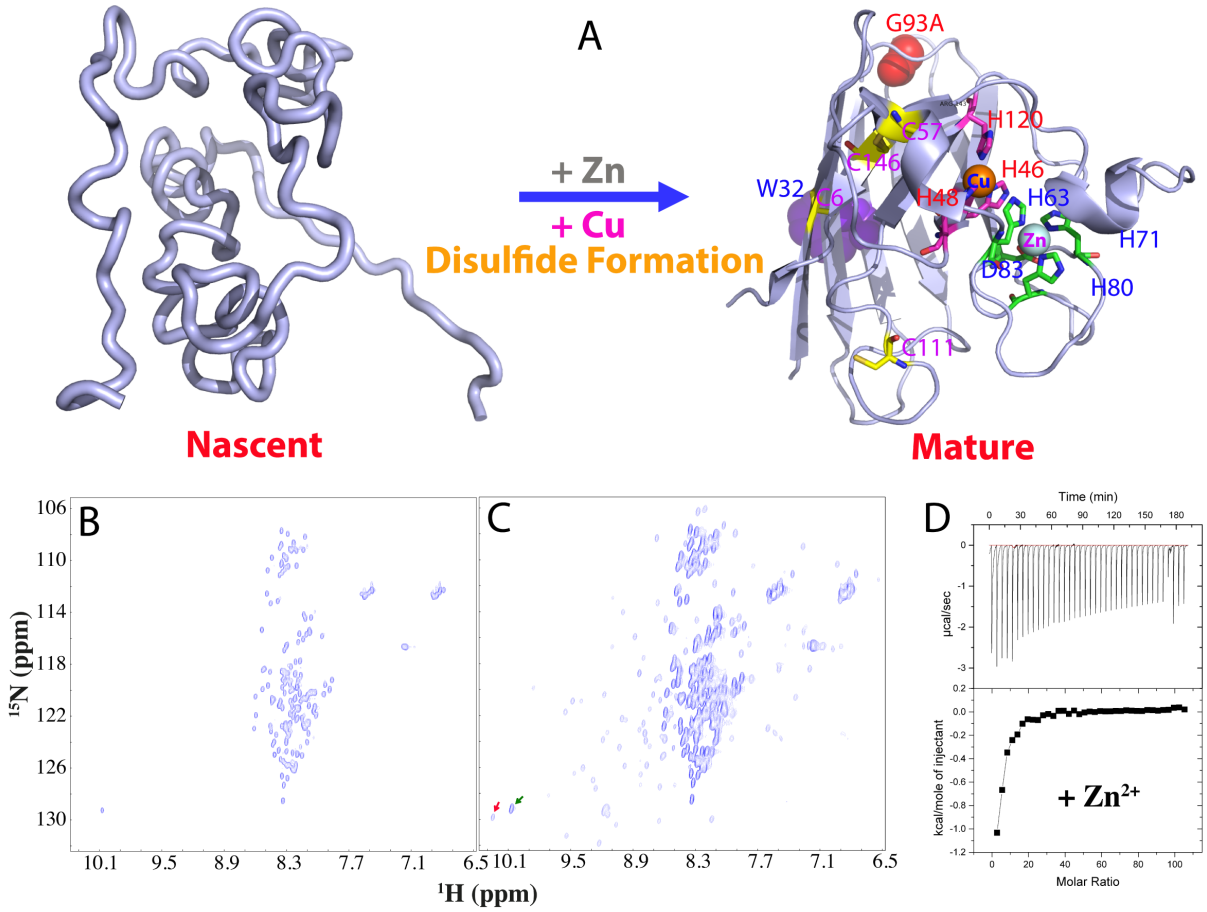

Fig. 1. Zn^{2+} binds and initiates folding of the nascent hSOD1.
(A) Schematic representation of the maturation process of hSOD1 from the unfolded nascent state to mature subunit. Mature hSOD1 is represented by the monomeric subunit of the dimeric crystal structure of hSOD1 (PDB ID of 2C9V). Residues critical for binding metal cofactors are labeled. (B) Two-dimensional ^{1}H-^{15}N NMR HSQC spectrum of the nascent hSOD1 of the WT sequence without metalation and disulfide bridge. (C) HSQC spectrum of the nascent hSOD1 in the presence of zinc at a ratio of 1:20 (hSOD1:zinc). Green arrow is used for indicating HSQC peak of the Trp32 ring proton resulting from the unfolded state while red arrow for that from the folded hSOD1. (D) (Upper) ITC profiles of the interactions of the unfolded hSOD1 state with Zn^{2+}, and (Lower) integrated values for reaction heats with subtraction of the corresponding blank results normalized against the amount of ligand injected versus the molar ratio of hSOD1:Zn.

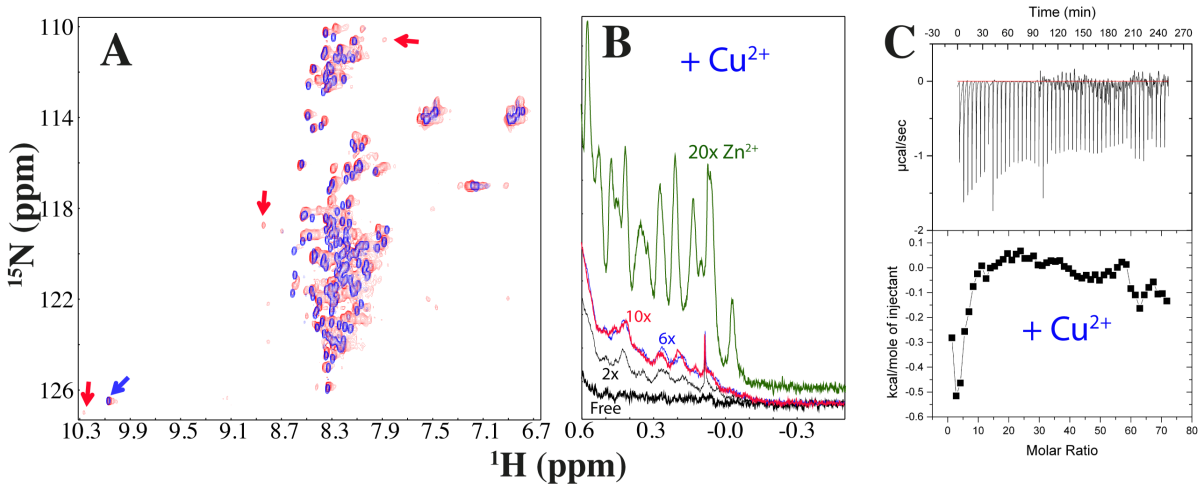

Fig. 2. Copper binds the nascent hSOD1.
(A) Superimposition of HSQC spectra of the nascent hSOD1 (blue) and in the presence of Cu^{2+} at a molar ratio of 1:10 (red). The blue arrow is used for indicating the HSQC peak of Trp32 ring proton characteristic of the unfolded state and red ones for some peaks characteristic of the partially-folded form. (B) The up-field 1D NMR peaks characteristic of the partially-folded hSOD1 (-0.5-0.62 ppm) in the absence and in the presence of Cu^{2+} at different molar ratios. (C) (Upper) ITC profiles of the interactions of the nascent hSOD1 with Cu^{2+}, and (Lower) integrated values for reaction heats with subtraction of the corresponding blank results normalized against the amount of ligand injected versus the molar ratio of hSOD1:Cu.

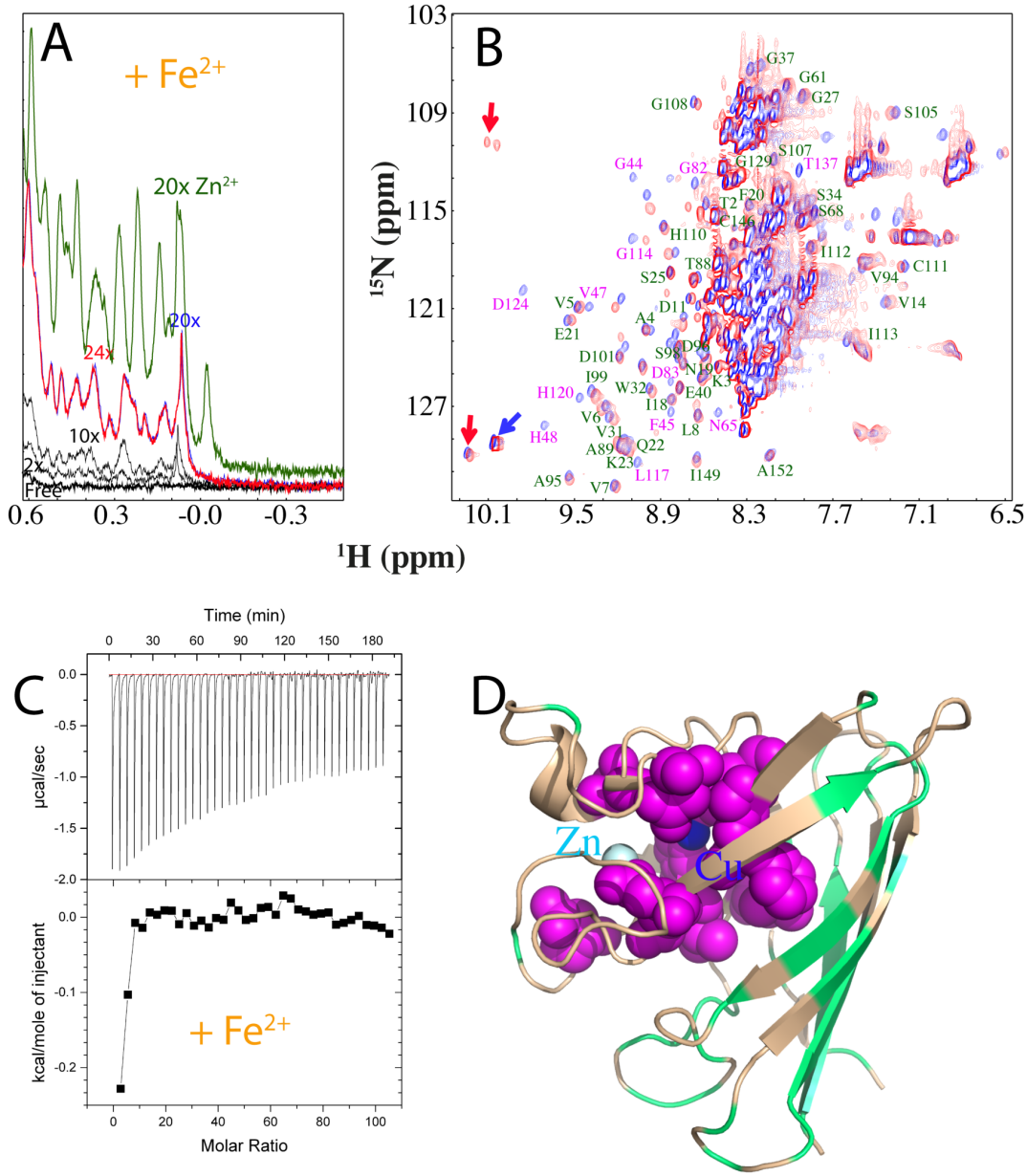

Fig. 3. Fe^{2+} has the Zn^{2+}-like ability to bind and induce folding.
(A) Up-field 1D NMR peaks characteristic of the nascent hSOD1 (-0.5-0.62 ppm) in the absence and in the presence of Fe^{2+} at different molar ratios. (B) Superimposition of HSQC spectra of hSOD1 in the presence of Zn^{2+} (blue) and Fe^{2+} (red). The labels of the sequential assignments for some well-resolved HSQC peaks are in green if the peaks are largely superimposable but in pink if the peaks are largely different in both forms. (C) (Upper) ITC profiles of the interactions of the nascent hSOD1 with Fe^{2+}, and (Lower) integrated values for reaction heats with subtraction of the corresponding blank results normalized against the amount of ligand injected versus the molar ratio of SOD1:Fe. (D) The monomer structure of hSOD1 (1PU0) with the residues displayed in pink spheres if their HSQC peaks largely different and colored in green if their HSQC peaks highly superimposable in two forms.

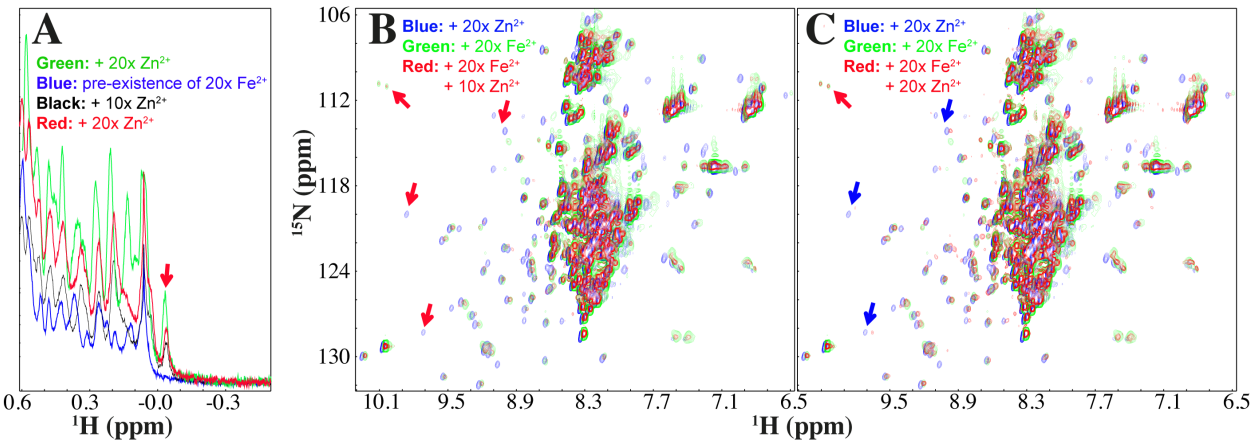

Fig. 4. Fe^{2+} and Zn^{2+} might have partly overlapped binding pockets.
(A) Up-field 1D NMR peaks (-0.5-0.62 ppm) of hSOD1 in the presence of 20x Zn^{2+} (green), 20x Fe^{2+} (blue), addition of 10x Zn^{2+} into the sample in the pre-existence of 20x Fe^{2+} (black); and addition of 20x Zn^{2+} into the sample in the pre-existence of 20x Fe^{2+} (red). Red arrow is used for indicating Zn^{2+}-specific 1D peak. (B) Superimposition of HSQC spectra of hSOD1 in the presence of 20x Zn^{2+} (blue), in the presence of 20x Fe^{2+} (green), and in the presence of both 20x Fe^{2+} and 10x Zn^{2+}. (C) Superimposition of HSQC spectra of hSOD1 in the presence of 20x Zn^{2+} (blue), in the presence of 20x Fe^{2+} (green), and in the presence of both 20x Fe^{2+} and 20x Zn^{2+}. Red arrows are used for indicating Fe^{2+}-specific HSQC peaks while blue arrows for Zn^{2+}-specific peaks.

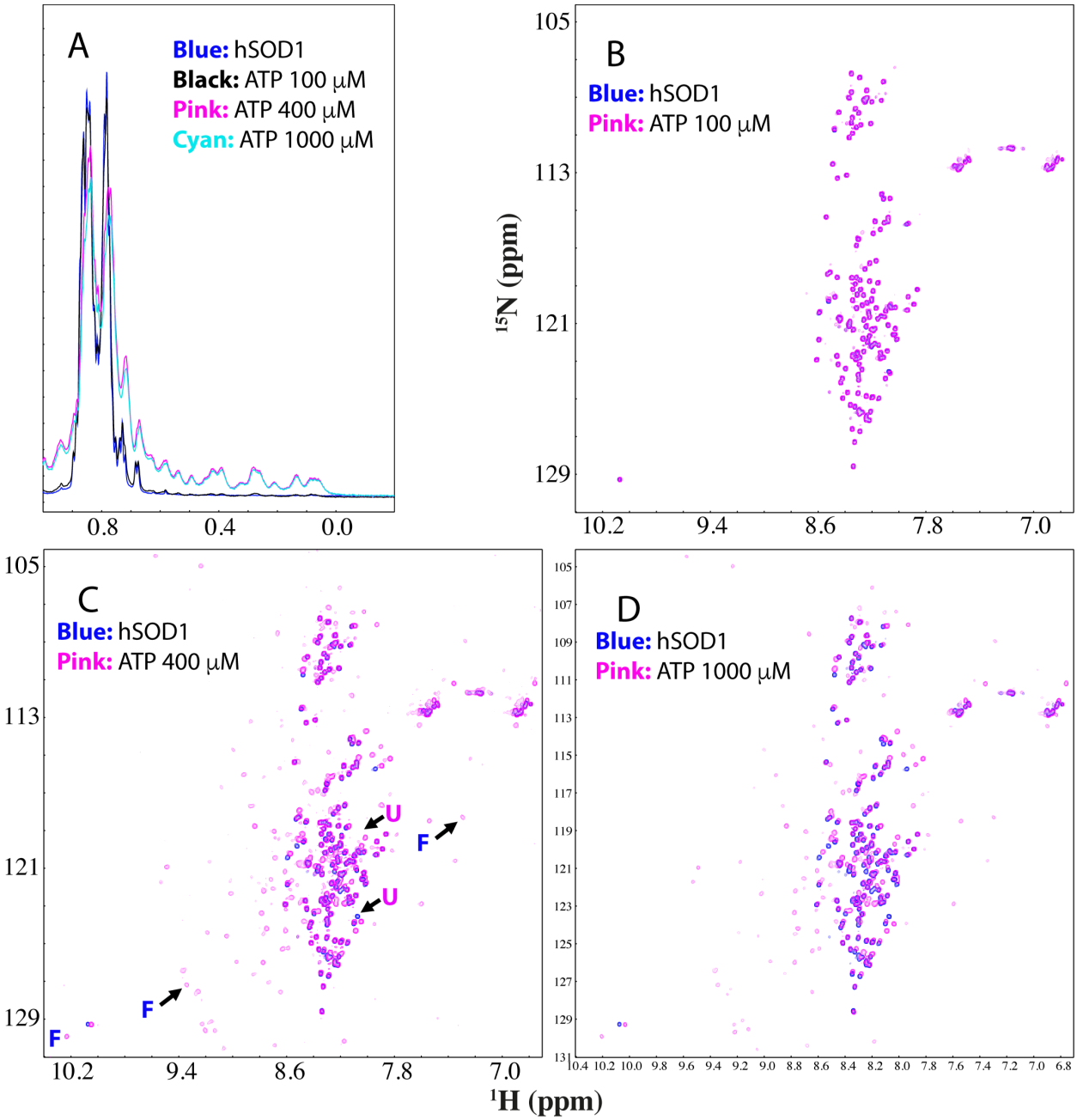

Fig. 5. ATP induces folding of the nascent hSOD1.
(A) Up-field 1D NMR spectra of ^{15}N-labeled hSOD1 at a concentration of 50 μM in the presence of ATP at different ratios. (B) Superimposition of HSQC spectra of ^{15}N-labeled hSOD1 in the absence (blue) and in the presence of ATP at 1:2 (pink). (C) Superimposition of HSQC spectra of ^{15}N-labeled hSOD1 in the absence (blue) and in the presence of ATP at 1:8 (pink). (D) Superimposition of HSQC spectra of ^{15}N-labeled hSOD1 in the absence (blue) and in the presence of ATP at 1:20 (pink).

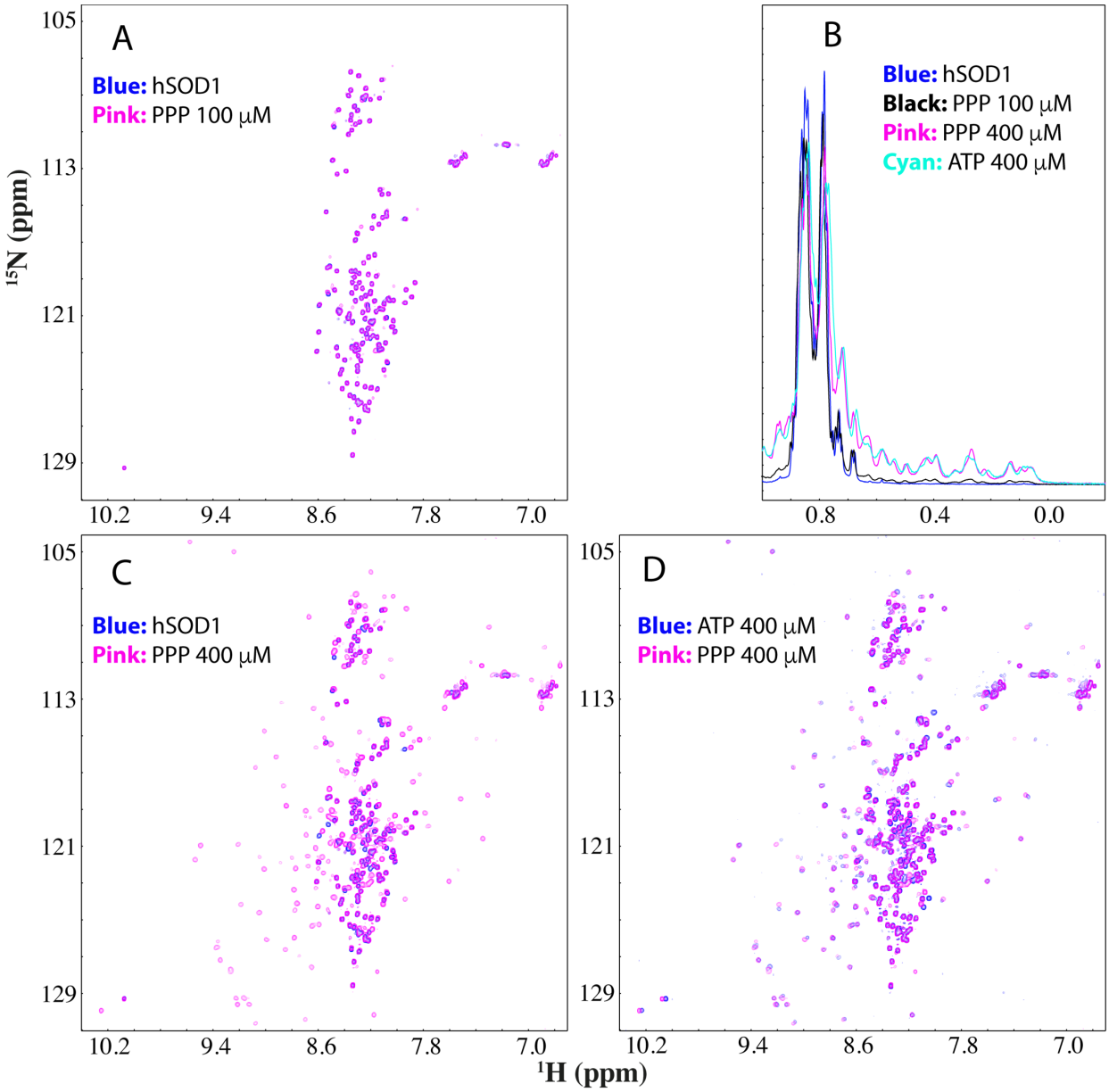

Fig. 6. PPP induces folding of the nascent hSOD1.
(A) Superimposition of HSQC spectra of ^{15}N-labeled hSOD1 at a concentration of 50 μM in the absence (blue) and in the presence of PPP at 1:2 (pink). (B) Up-field 1D NMR spectra of hSOD1 in the presence of PPP at different ratios. (C) Superimposition of HSQC spectra of ^{15}N-labeled hSOD1 in the absence (blue) and in the presence of PPP at 1:8. (D) Superimposition of HSQC spectra of ^{15}N-labeled hSOD1 in the presence of ATP at 1:8 (blue) and PPP at 1:8 (pink).

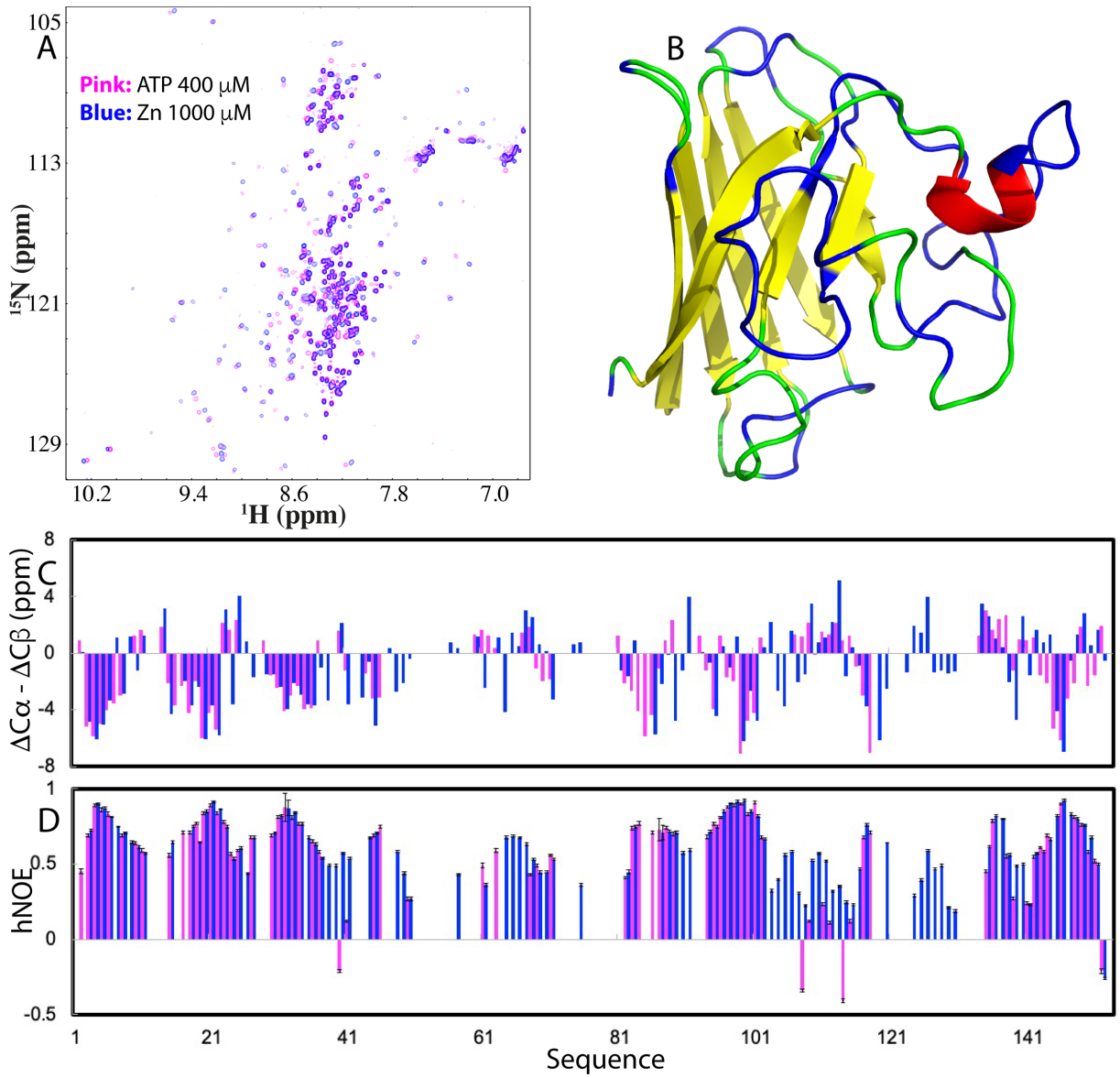

Fig. 7. Comparison of NMR conformations of the ATP- and Zn-induced folded state. (A) Superimposition of HSQC spectra of ^{15}N-labeled hSOD1 in the presence of ATP at 1:8 (blue) and in the presence of zinc cation (pink) at 1:20. (B) NMR structure of C6A/C111S with the unassigned residues of the ATP-induced folded state colored in blue due to missing or overlapping resonances. (C) Residue specific (ΔCα–ΔCβ) chemical shifts of the ATP-induced (purple) and Zn^{2+}-induced (blue) folded states of hSOD1. (D) $\{^{1}H\}$–^{15}N heteronuclear steady-state NOE (hNOE) of the ATP-induced (purple) and Zn^{2+}-induced (blue) folded states of hSOD1.

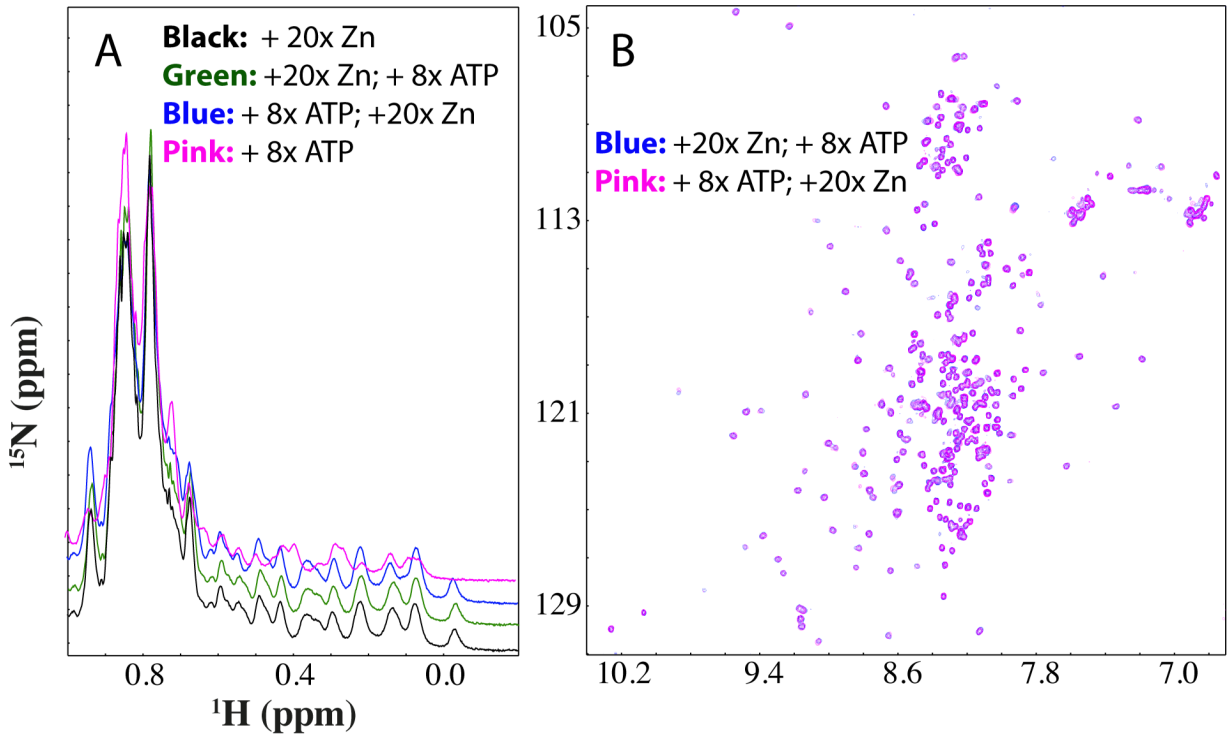

Fig. 8. ATP and Zn interplay in inducing folding of the nascent hSOD1.
(A) Up-field 1D NMR spectra of hSOD1 in the presence of zinc at 1:20 (black) and with further addition of ATP at 1:8 (green) as well as in the presence of ATP at 1:8 (purple) and with further addition of zinc at 1:20 (blue). (B) Superimposition of HSQC spectra of ^{15}N-labeled hSOD1 in the presence of zinc at 1:20 with further addition of ATP at 1:8 (blue) and in the presence of ATP at 1:8 with further addition of zinc at 1:20 (purple).

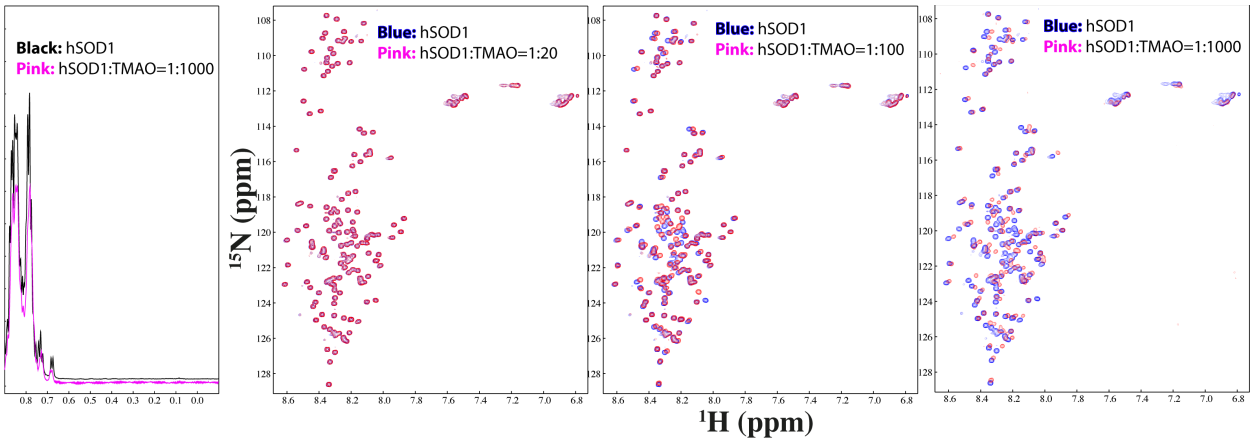

Fig. 9. TMAO fails to induce folding but triggers aggregation.
Up-field 1D and HSQC spectra of hSOD1 at a concentration of 50 μM in the presence of TMAO at different ratios.